Advances in Science and Technology
Research Journal

Advances in Science and Technology Research Journal, 2026, 20(9), 108–125
https://doi.org/10.12913/22998624/221816
ISSN 2299-8624, License CC-BY 4.0

Received: 2026.04.29
Accepted: 2026.06.22
Published: 2026.08.01

Nonlinear buckling and post-buckling response of steel trusses under localized fire exposure

Van Dat Pham[1], Ngoc Tien Dao[1*]

[1] Faculty of Civil Engineering, Hanoi Architectural University, Hanoi, Vietnam
* Corresponding author's e-mail: tiendn@hau.edu.vn

ABSTRACT

This paper develops a nonlinear finite element framework for buckling and post-buckling of steel dome trusses under combined mechanical loads and non-uniform temperature fields from localized fires. A weak coupling sequential strategy using McCaffrey's plume model with Gaussian lateral distribution determines the temperature field, which is then mapped onto the structural model. Fire location is parameterized by polar coordinates . The Updated Lagrangian (UL) formulation accounts for large displacements, thermal expansion, and temperature-dependent degradation of steel properties per Eurocode 3. The generalized displacement control (GDC) method traces full equilibrium paths. Validation against published results shows good agreement. Parametric study on an S275 steel truss under five fire scenarios (FS1–FS5) reveals that a fire at the dome center (FS1) increases the critical load by up to 109% due to arching, while a fire at the boundary (FS5) reduces it by approximately 4% – the most hazardous scenario. Elastoplastic analysis consistently yields lower critical loads than elastic analysis. These findings provide practical guidance for performance-based fire design of large-span steel dome trusses, highlighting that fires near the boundary are more dangerous than those near the center.

Keywords: steel truss, localized fire, nonlinear buckling, post-buckling, McCaffrey plume, Eurocode 3.

INTRODUCTION

Steel truss structures, particularly large-span latticed dome trusses, are widely employed in public buildings such as sports arenas, exhibition centers, and airports. One of the most critical design scenarios is fire, wherein the combined effects of mechanical loads and the non-uniform temperature field induced by a localized fire can lead to nonlinear instability and post-buckling failure.

Existing studies have primarily focused on uniformly distributed temperature fields or simplified thermal loadings [1–3]. Specifically, [2] investigated the instability of latticed dome trusses under uniform temperature conditions using a two-stage finite element procedure combined with the generalized displacement control (GDC) method. Full-scale experimental tests on steel roof trusses [4] and dynamic response analyses [5] have revealed differences between localized and traveling fire scenarios. Experimental studies by [6, 7] demonstrated that the behavior of truss members depends on the temperature distribution and joint configuration. [8] developed a simplified method showing that temperature effects on diagonal members most significantly reduce the load-carrying capacity of the truss. [9] indicated that considering both geometric and material nonlinearities simultaneously yields substantially lower critical loads.

In the field of nonlinear structural analysis, recent studies have focused on the effects of eccentric loads, temperature fields, and geometric imperfections. Specifically, [10] proposed an efficient numerical method based on the Levenberg–Marquardt algorithm to analyze the geometrically nonlinear behavior of beams subjected to combined eccentric compressive loads and thermal effects. For space truss structures, [11] and [12] developed hybrid finite element formulations to predict post-buckling behavior and dynamic responses accounting for initial member length imperfections, demonstrating significant influences on the limit load. Furthermore, [13] and [14] indicated that elastic support stiffness plays a crucial role in the static and dynamic stability of imperfect arch trusses and planar steel trusses. Finally, [15] introduced the p-Stochastic Global Optimization Algorithm (p-SGOA), showing that even small variations in member lengths can substantially enhance the critical load without altering the weight or original design shape of the truss. These findings offer practical insights for the design and stability assessment of skeletal structures subjected to combined loading effects.

Nevertheless, these studies suffer from several limitations: (i) the uniform temperature assumption does not reflect realistic localized fire scenarios; (ii) thermo-mechanical interactions are often treated in a decoupled manner; (iii) the influence of fire location on post-buckling behavior remains largely unexplored; (iv) most existing models do not simultaneously account for large displacements, degradation of mechanical properties according to EC3 (Eurocode 3 1993) [16], and elastoplastic behavior.

Recently, considerable efforts have been made to improve the understanding of steel structures under fire conditions. Regarding material behavior, the EC3 reduction factors for hot-rolled steel may not be directly applicable to cold-formed steel [17]. Regarding structural behavior, experimental tests on tubular steel trusses under axial loading in fire conditions [18] and parametric studies on square hollow section T-joints [19] have been conducted. The effects of non-uniform temperature fields have begun to receive attention, including thermal shielding effects [20] and coupled CFD-FE analyses of long-span truss beams exposed to traveling fires [21]. Most recently, proposed revisions to European standards for the fire design of slender steel beams have been published [22]. Experimental investigations on the collapse of industrial warehouse roof truss systems under fire exposure have also been analyzed [23].

To address the aforementioned gaps, this paper proposes a comprehensive nonlinear finite element (FE) framework for analyzing the stability and post-buckling response of steel trusses subjected to thermo-mechanical loading with non-uniform temperature fields arising from localized fires. The main contributions include: (i) a sequential weak-coupling analysis strategy; (ii) a non-uniform temperature field model based on McCaffrey's plume [24] combined with a Gaussian lateral distribution; (iii) a fire location parameterization method using polar coordinates; (iv) a unified nonlinear FE formulation accounting for large displacements (Lagrangian description) and temperature-dependent degradation of material properties according to EC3; (v) the GDC method to trace the complete equilibrium path. The theoretical framework is validated against published results for a uniform temperature field [2] (Example 1). Subsequently, a parametric study (Example 2) is conducted on an S275 steel tubular latticed dome truss under five fire scenarios ranging from the dome center ($r_Q = 0$) to the boundary ($r_Q = R$). The main novelty of the paper is the combined use of a McCaffrey plume-based localized fire model, Gaussian lateral temperature distribution, fire-location parameterization, and nonlinear finite element post-buckling analysis of steel dome trusses. The paper is organized as follows: Section 2 presents the temperature field model; Section 3 presents the equilibrium equations; Section 4 presents numerical examples; Section 5 provides conclusions.

CLASSIFICATION AND MODELING OF THE STEEL TRUSS PROBLEM UNDER LOCALIZED FIRE EXPOSURE

The problem of steel trusses subjected to localized fire is complex and challenging. The main challenges include: (i) correctly classifying the thermo-mechanical problem under consideration as either weakly coupled or strongly coupled; (ii) developing an appropriate model and computational procedure for the non-uniform temperature field; (iii) modeling heat transfer within the steel truss structure; (iv) handling arbitrary fire locations using a parameterization method and establishing an analysis procedure for trusses under localized fire, wherein geometric nonlinearities, material nonlinearities, and the temperature-induced degradation of steel mechanical properties must be accounted for. These challenges are addressed in detail in the following subsections.

Problem classification

In deformable solid mechanics and finite element analysis, coupled thermo-mechanical problems are classified based on the degree of interaction between the temperature and mechanical fields:

1) Weak coupling: The temperature field influences the mechanical field through thermal expansion, but deformations and stresses do not significantly affect the temperature distribution. Such problems are typically solved using a sequential strategy: the heat transfer problem is solved first, and the resulting temperature field is subsequently applied as thermal loading in the mechanical analysis.
2) Strong coupling (or full coupling): Two-way interaction exists, where deformations and stresses may generate heat (thermoplasticity, viscoelasticity, thermoelasticity). The problem must be solved simultaneously or through tight iteration between the two fields.

In the present study, the problem of „Nonlinear buckling and post-buckling response of steel trusses under localized fire exposure" belongs to the weak coupling class. Accordingly, a sequential solution strategy is adopted: the temperature field is first determined using the McCaffrey plume model [24] and then mapped onto the mechanical model for nonlinear buckling and post-buckling analysis.

Procedure for calculating heat transfer from a localized fire to individual truss members

To simulate the non-uniform temperature field induced by a fire, three main approaches are available:

- empirical models: the McCaffrey plume model [24] provides predictive formulas for temperature and velocity along the centerline of the fire plume as functions of heat release rate and flame height.
- semi-empirical models: two-zone models [25], [26] divide the fire compartment into an upper hot gas layer and a lower cold layer, enabling description of vertical temperature non-uniformity within the enclosure.
- CFD models: CFD software, such as the fire dynamics simulator (FDS) developed by NIST

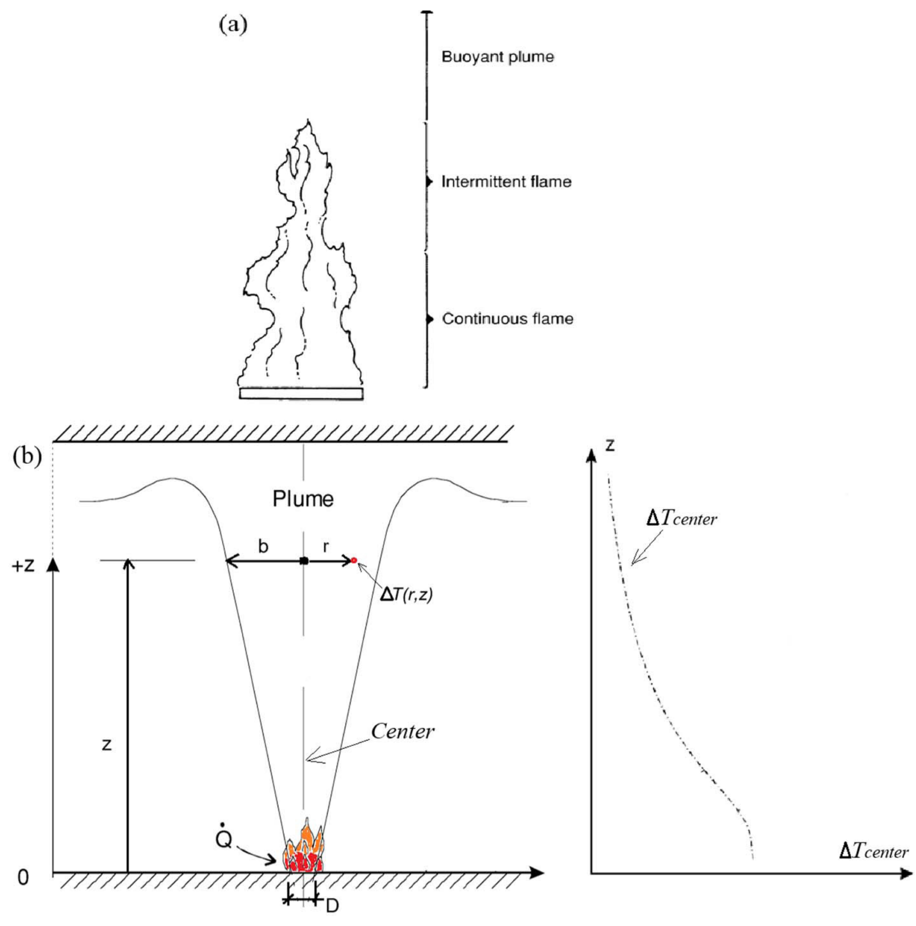

Figure 1. McCaffrey plume model: (a) the three zones of the axisymmetric buoyant plume; (b) some of the characteristics of a buoyant axisymmetric plume [24]

[27], can simulate detailed three-dimensional temperature fields.

To strike a balance between accuracy and computational efficiency for parametric studies, the present study adopts an approach that combines the McCaffrey plume empirical model [24] with the finite element method (to be established in Section 3) for the simultaneous simulation of the temperature field and structural response. Based on this, a generalized temperature distribution function $\Delta T(\dot{Q}, D, x, y, z)$ is developed, expressing the temperature field dependence on input parameters including the total heat release rate of the fire source $\dot{Q}$, the characteristic diameter of the fire source D, and spatial coordinates (x, y, z). The present study employs the McCaffrey plume model [24] (see Figure 1) as it is suitable for the nature of fires expected in large-span steel domed sports facilities (e.g., multi-purpose arenas).

McCaffrey [24] used experimental data and dimensional analysis to establish relationships for buoyant plumes, including upward velocity and temperature. He divided the plume into three zones, as shown in Figure 1a: the continuous flame zone, the intermittent flame zone, and the plume zone. The equation for the centerline temperature rise $\Delta T_{center}(z)$ at elevation z (see Figure 1(b)) is as follows:

$$\Delta T_{center}(z) = (T_{center} - T_0) = \\ = \left(\frac{\kappa}{0.9\sqrt{2g}}\right)^2 \cdot \left(\frac{z}{\dot{Q}^{2/5}}\right)^{2\eta-1} \cdot T_0 \tag{1}$$

where: $T_0 = 293\ K$ and $g = 9.81\ \text{m/s}^2$ are approximate ambient air properties; the constants η and κ vary with the three zones as given in Table 1. The centerline and ambient temperatures are T_{center} and T_0, respectively, in Kelvin $[K]$; z is in meters [m]; $\dot{Q}$ is in kilowatts $[kW]$.

Note that, according to [25], the plume radius $b(z)$ in Figure 1(b) is defined by a spread angle of approximately 15° from the vertical. The fire source diameter D in Figure 1b is in meters [m], [25]. The lateral distribution of the temperature rise $\Delta T(r, z)$ on a horizontal plane at elevation z (see Figure 1b) is expressed as a Gaussian distribution:

$$\Delta T(r,z) = \Delta T_{center}(z) \cdot e^{\frac{-r^2}{(\sigma_{\Delta T})^2}} = \\ = \Delta T_{center}(z) \cdot e^{\frac{-r^2}{(1.201b(z))^2}} \tag{2}$$

where: r is the radial distance from the plume centerline to the point of interest. According to [25], for Gaussian distributions, $\sigma_{\Delta T} = 1.201b(z)$ is recommended as it agrees well with experimental measurements for fire plumes.

Assuming the input parameters are known, including the floor-plan coordinates of the fire center, fire diameter D, total heat release rate $\dot{Q}$, and ambient air properties $T_0[K]$ and $g[\text{m/s}^2]$, a procedure for calculating the temperature T within a truss member located in the plume is proposed based on Equations 1 and 2 and Table 1:

1) Identify the three zones (continuous flame, intermittent flame, and plume) according to Table 1.
2) Determine the location (r, z) of the truss member's centroid and identify in which of the three zones it lies. Compute the centerline temperature rise $\Delta T_{center}(z)$ using Equation 1.
3) Compute the plume radius $b(z)$ assuming a 15° spread angle from the vertical. Compute the temperature rise $\Delta T(r, z)$ in the truss member using Equation (2), then obtain the member temperature as $T = \Delta T(r, z) + T_0$.

Table 1. Constants in McCaffrey's plume equations, [24]

Region	Parameter	η	κ
Continuous	< 0.08	1/2	6.8
Intermittent	0.08–0.2	0	1.9
Plume	> 0.2	-1/3	1.1

Heat transfer analysis procedure for the entire steel truss structure

Since steel trusses consist of slender members, a beam/truss element model with the assumption of a uniform temperature across the cross-section is appropriate. For steel tubes with high thermal conductivity, this assumption is particularly reasonable. The heat transfer analysis procedure for the entire truss structure is as follows:

Perform heat transfer analysis from the McCaffrey plume to each individual member. The result is a spatially varying temperature field, denoted $T(r, z)$ or $T(x, y, z)$, for each truss element.

This temperature field is then mapped and assigned as input to the global truss structural model. Finally, the problem of analyzing the buckling and post-buckling behavior of the steel truss under combined mechanical and thermal loads is solved using the finite element method.

Handling arbitrary fire locations – parameterization method and analysis procedure

For an axisymmetric domed steel truss, the location of the fire center on the floor plan is defined using polar coordinates (r_Q, θ), where r_Q is the distance from the dome center to the fire center, and θ is the angle between the radius vector r_Q and the global X-axis of the truss (Figure 2). Fire location scenarios are considered within one quadrant of the floor plan, specifically with $\theta = \pi/4$. The radial distance r_Q takes the values listed in Table 2, where R denotes the radius of the dome truss on the floor plan. Based on the foregoing analysis, the proposed procedure for analyzing the problem of nonlinear buckling and post-buckling response of steel trusses under localized fire exposure is as follows:

- Input parameter definition: Establish truss geometry, mechanical loads, and fire parameters (radius, height, nodal coordinates; mechanical loads; fire location, heat release rate, fire diameter).
- McCaffrey plume fire simulation: Compute the plume centerline temperature using Equation 1. Divide the plume into three zones: continuous flame, intermittent flame, and plume. Compute the temperature T in each truss member.
- Heat transfer analysis on the structure: Use the finite element method to map the temperature field onto the truss members. Assign the temperature $T(r, z)$ to each element, assuming a uniform temperature across the cross-section.
- Nonlinear mechanical analysis: Solve the buckling and post-buckling problem using the nonlinear finite element method. Account for geometric nonlinearity and material nonlinearity, and employ the GDC method.
- Post-processing and evaluation: Evaluate the analysis results to determine the critical load and the influence of fire location. The results to be presented include: (i) load–displacement curves; (ii) critical loads; (iii) influence of fire location.

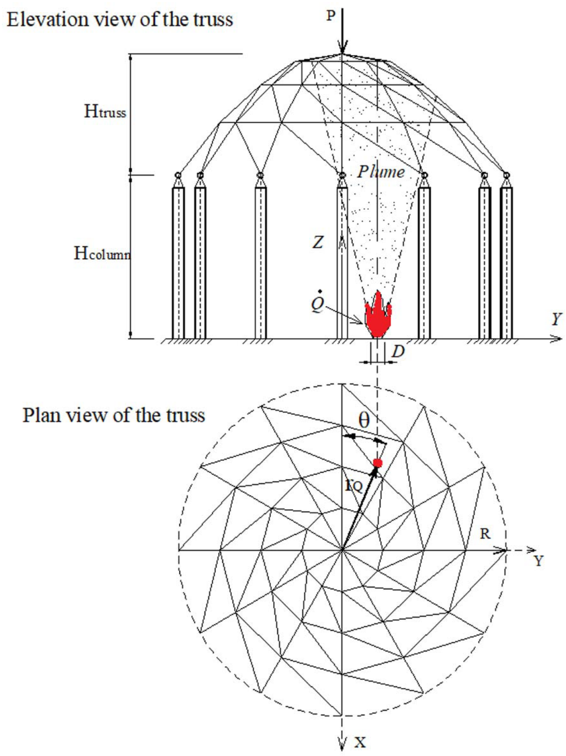

Figure 2. Parameterization of fire center location on the floor plan using polar coordinates (r_Q, θ)

EQUILIBRIUM EQUATIONS OF A TRUSS MEMBER AND THE STEEL TRUSS SYSTEM UNDER THERMO-MECHANICAL LOADING

A spatial steel truss element model under thermo-mechanical loading is developed, accounting simultaneously for thermal expansion

Table 2. Parametric scenarios investigated

Scenario	Fire center location (r_Q, θ)	Description
FS1	$r_Q = 0$	Perfectly symmetric
FS2	$r_Q = R/4$, $\theta = \pi/4$	Near dome center
FS3	$r_Q = R/2$, $\theta = \pi/4$	Intermediate
FS4	$r_Q = 3R/4$, $\theta = \pi/4$	Near dome boundary
FS5	$r_Q = R$, $\theta = \pi/4$	At dome boundary

of the member and the degradation of steel material properties such as elastic modulus and yield strength at elevated temperatures. Thus, geometric nonlinearity (due to large displacements) and material nonlinearity (elastoplastic model) are both considered in the present study. Based on the Updated Lagrangian (UL) formulation, the equilibrium equations and their incremental forms for a truss member and the entire truss system are derived. The GDC method is employed to solve the system of nonlinear equilibrium equations, from which the equilibrium path as well as the critical load and critical temperature of the truss are determined.

Mechanical properties of steel at elevated temperatures

In this study, two material models are considered: elastic (EL) and elastoplastic (EP). At elevated temperatures, both the elastic modulus and yield strength of steel degrade. The reduction factors are provided by EC3 [16] as shown in Figure 3 and Table 3.

Equilibrium equation of a truss member under thermo-mechanical loading

To address geometric nonlinearity within the Lagrangian framework, three configurations are considered (Figure 4). Let C_0 be the initial configuration, C_1 the previously computed configuration, and C_2 the current configuration to be computed. The physical quantities—temperature, length, cross-sectional area, elastic modulus, and yield stress—in configuration C_0 are denoted by (${}^0T$, ${}^0L$, ${}^0A$, ${}^0E$, ${}^0\sigma_y$); similarly for configurations C_1(${}^1T$, ${}^1L$, ${}^1A$, ${}^1E$, ${}^1\sigma_y$) and C_2 (${}^2T$, ${}^2L$, ${}^2A$, ${}^2E$, ${}^2\sigma_y$). The axial forces at configurations C_1 and C_2 are ${}^1_1F_x$ and ${}^2_2F$, respectively (Figure 5). In the Total Lagrangian (TL) formulation, the equilibrium equation of the element in configuration C_2 is constructed by choosing C_0 as the reference configuration; if the reference configuration is chosen as C_1, the corresponding formulation is the UL. The notation (${}^m_nQ$) for physical quantities is interpreted as follows: the left superscript ‚*m*' denotes the configuration in which the quantity occurs, and the left subscript ‚*n*' denotes the

Table 3. Reduction factors of the mechanical properties of steel as a function of temperature (according to EC3). (Yield strength reduction factor, $k_{y,\theta} = \sigma_y(T)/\sigma_{y,20}$; Young's modulus reduction factor, $k_{E,\theta} = E(T)/E_{20}$)

Temp. (°C), T	20	200	400	600	800	1000	1200
Yield strength reduction factor, $k_{y,\theta}$	1.000	1.000	1.000	0.470	0.110	0.040	0.000
Young's modulus reduction factor, $k_{E,\theta}$	1.000	0.900	0.700	0.310	0.090	0.045	0.000

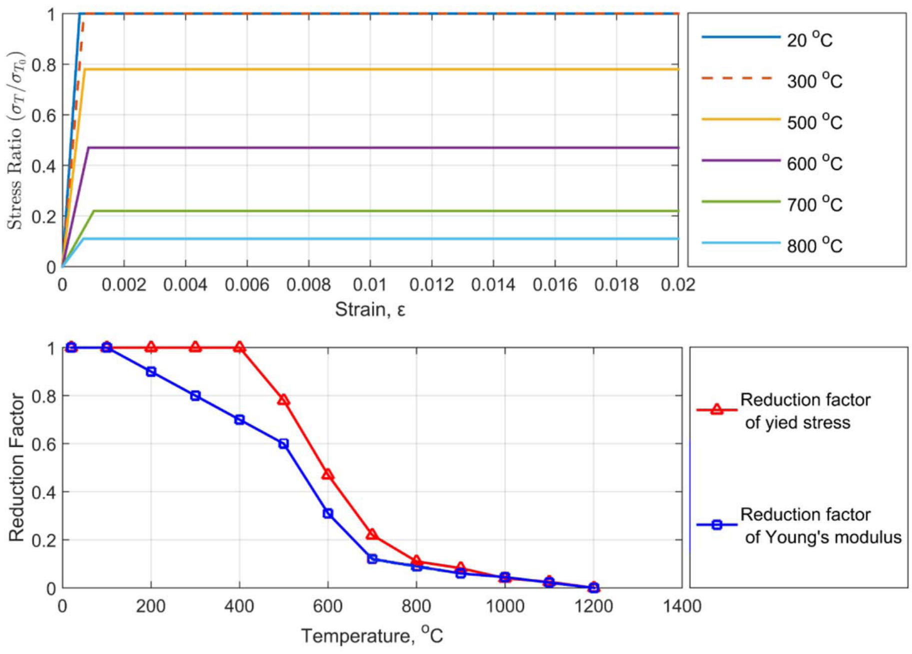

Figure 3. Elastoplastic metarials and reduction factors from EC3 [16]

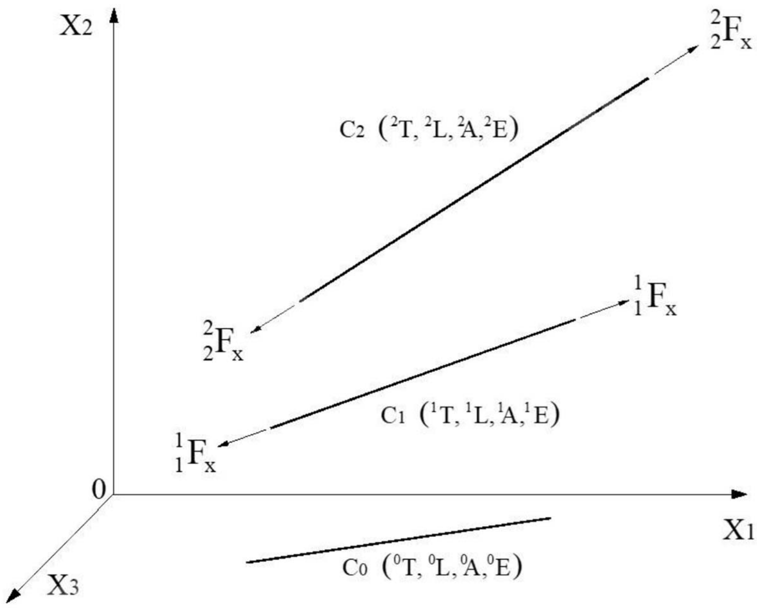

Figure 4. Configurations C_0, C_1, and C_2 in the Lagrangian method for handling large displacements of 3D truss members subjected to mechanical and thermal loads

configuration with respect to which the quantity is measured. [2]

Let α denote the coefficient of thermal expansion of steel, $\Delta T = 2T - 0T$ the temperature difference, and $T_m = ({}^2T + {}^0T)/2$ the mean temperature. According to [28], the thermal expansion coefficient is calculated as $\alpha = [11.09 + 0.0062 \cdot T_m(°C)] \cdot 10^{-6}(1/C°)$. The thermal strain of the member in C_2 is:

$$ {}^2_0\varepsilon_{thermal} = \alpha\Delta T = \alpha({}^2T - {}^0T) \tag{3} $$

If Green's strain is chosen for the analysis, the total strain of the member is:

$$ {}^2_0\varepsilon_{total} = \frac{({}^2L)^2 - ({}^0L)^2}{2 \cdot L^2}. \tag{4} $$

Since the total strain ${}^2_0\varepsilon_{total}$ is the sum of the thermal strain ${}^2_0\varepsilon_{thermal}$ and the mechanical strain ${}^2_0\varepsilon_{mech}$, which is related to the mechanical stress ${}^2_0\sigma$, the mechanical strain is written as:

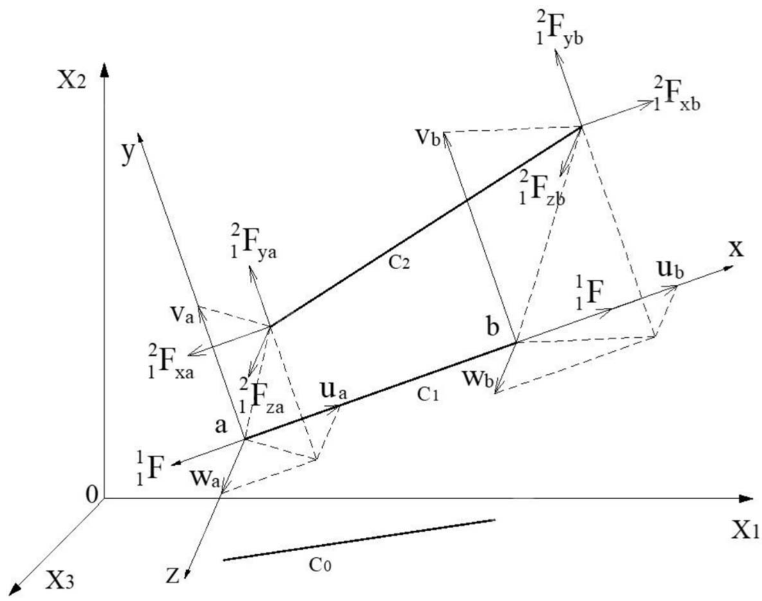

Figure 5. Displacement of a truss member from configuration C_1 to C_2 in space

$$ {}_{0}^{2}\varepsilon_{mech} = {}_{0}^{2}\varepsilon_{total} - {}_{0}^{2}\varepsilon_{thermal} = \frac{({}^{2}L)^{2}-({}^{0}L)^{2}}{2\cdot L^{2}} - \alpha({}^{2}T - {}^{0}T). \quad (5) $$

The second Piola–Kirchhoff stress ${}_{0}^{2}\sigma$ is related to the mechanical strain ${}_{0}^{2}\varepsilon_{mech}$ as:

$$ {}_{0}^{2}\sigma = ({}^{2}E)\cdot {}_{0}^{2}\varepsilon_{mech} \quad (6) $$

Assuming the cross-sectional area remains unchanged (${}^{0}A = {}^{1}A = {}^{2}A$), the Cauchy stress ${}_{2}^{2}\sigma$ (true stress in C_2) relates to the second Piola–Kirchhoff stress ${}_{0}^{2}\sigma$ as:

$$ {}_{2}^{2}\sigma = {}_{0}^{2}\sigma \cdot \frac{{}^{2}L}{{}^{0}L} \quad (7) $$

The axial force ${}_{2}^{2}F$ of the truss element in configuration C_2 is:

$$ {}_{2}^{2}F_{x} = {}_{2}^{2}\sigma \cdot A = {}_{0}^{2}\sigma \cdot \frac{{}^{2}L}{{}^{0}L} \cdot A \quad (8) $$

Substituting (5) and (6) into (8) yields:

$$ {}_{2}^{2}F_{x} = {}^{2}E \cdot A \cdot \left(\frac{({}^{2}L)^{2}-({}^{0}L)^{2}}{2\cdot L^{2}} - \alpha({}^{2}T - {}^{0}T)\right)\cdot \frac{{}^{2}L}{{}^{0}L} \quad (9) $$

Equation 9 is the expression for calculating the axial force of a truss member accounting for temperature effects.

To derive the incremental equilibrium equation of the truss member within the finite element framework, the reference configuration is chosen as C_1 corresponding to the UL formulation (Figure 5). The internal force vector (${}_{1}^{2}\boldsymbol{F}$) at nodes *'a'* and *'b'* in C_2 referenced to C_1 is decomposed into six components:

$$ {}_{1}^{2}\boldsymbol{F} = \left\{{}_{1}^{2}F_{xa}, {}_{1}^{2}F_{ya}, {}_{1}^{2}F_{za}, {}_{1}^{2}F_{xb}, {}_{1}^{2}F_{yb}, {}_{1}^{2}F_{zb}\right\}^{T} \quad (10) $$

where:

$$ {}_{1}^{2}F_{xa,xb} = {}_{2}^{2}F\frac{\partial({}^{2}L)}{\partial u_{a,b}};\ {}_{1}^{2}F_{ya,yb} = $$

$$ = {}_{2}^{2}F\frac{\partial({}^{2}L)}{\partial v_{a,b}};\ {}_{1}^{2}F_{za,zb} = {}_{2}^{2}F\frac{\partial({}^{2}L)}{\partial w_{a,b}}. $$

The nodal displacement vector is $\{u_a, v_a, w_a, u_b, v_b, w_b\}^{T}$, and the member length (${}^{2}L$) is a nonlinear function of the displacement variables, specifically:

$$ {}^{2}L = \sqrt{({}^{1}L + u_b - u_a)^{2} + (v_b - v_a)^{2} + (w_b - w_a)^{2}} \quad (11) $$

Expanding the vector (${}_{1}^{2}\boldsymbol{F}$) in a Taylor series about C_1 and neglecting higher-order infinitesimals:

$$ {}_{1}^{2}\boldsymbol{F} = {}_{1}^{2}\boldsymbol{F}|_{C_1} + \frac{\partial({}_{1}^{2}\boldsymbol{F})}{\partial \boldsymbol{u}}|_{C_1}\delta\boldsymbol{u} \quad (12) $$

where:

$$ \delta\boldsymbol{u} = \{u_a, v_a, w_a, u_b, v_b, w_b\}^{T}, {}_{1}^{2}\boldsymbol{F}|_{C_1} = {}_{1}^{1}\boldsymbol{F}. $$

Equation 12 can be rewritten in incremental form as:

$$ \boldsymbol{k}\delta\boldsymbol{u} = \boldsymbol{\Delta F} \quad (13) $$

where: $\boldsymbol{k} = \frac{\partial({}_{1}^{2}\boldsymbol{F})}{\partial \boldsymbol{u}}|_{C_1}$ is the tangent stiffness matrix at configuration C_1; $\Delta F = {}_{1}^{2}\boldsymbol{F} - {}_{1}^{1}\boldsymbol{F}$ is the incremental nodal internal force vector. The increment of nodal internal forces (ΔF) must balance the increment of nodal external forces $(\boldsymbol{\Delta p} = {}_{1}^{2}\boldsymbol{p} - {}_{1}^{1}\boldsymbol{p})$ [2]; therefore, Equation 13 becomes:

$$ \boldsymbol{k}\delta\boldsymbol{u} = \boldsymbol{\Delta p}. \quad (14) $$

Equilibrium equation of the truss system and selection of solution algorithm

Let $\boldsymbol{\Gamma}_{e}$ be the coordinate transformation matrix of the truss element. The relationships between vectors in the global and local coordinate systems are $\delta\boldsymbol{U}_{e} = \boldsymbol{\Gamma}_{e}^{T}\delta\boldsymbol{u}, \boldsymbol{\Delta P}_{e} = \boldsymbol{\Gamma}_{e}^{T}\boldsymbol{\Delta p}$. Equation 14 can then be rewritten as:

$$ \boldsymbol{\Gamma}_{e}^{T}\boldsymbol{k}\boldsymbol{\Gamma}_{e}\delta\boldsymbol{U}_{e} = \boldsymbol{\Gamma}_{e}^{T}\boldsymbol{\Delta p}\ \ or\ \ (\boldsymbol{\Gamma}_{e}^{T}\boldsymbol{k}\boldsymbol{\Gamma}_{e})\delta\boldsymbol{U}_{e} = \boldsymbol{P}_{e}. \quad (15) $$

Assembling the stiffness matrices, displacement vectors, and load vectors of individual elements in the global coordinate system according to the standard finite element procedure yields the incremental equilibrium equation for the truss system:

$$ \boldsymbol{K}\delta\boldsymbol{U} = \boldsymbol{\Delta P} \quad (16) $$

where:

$$ \boldsymbol{K} = \sum_{e}\boldsymbol{\Gamma}_{e}^{T}\boldsymbol{k}\boldsymbol{\Gamma}_{e};\ \delta\boldsymbol{U} = \sum_{e}\delta\boldsymbol{U}_{e};\ \boldsymbol{\Delta P} = \sum_{e}\boldsymbol{\Delta P}_{e}. $$

In the present study, the GDC method is employed to solve Equation 16. Details of the algorithm can be found in [29–31].

NUMERICAL EXAMPLES AND DISCUSSION

In this subsection, numerical examples are presented to validate and illustrate the proposed model for analyzing steel trusses under thermo-mechanical loading. The first example serves to verify the correctness of the nonlinear finite element model and the algorithm proposed in Section 3 through comparison with previous results. The second example is practically oriented, applying the theoretical framework of Section 2 in conjunction with the finite element model of Section 3 to a latticed steel dome truss subjected to a non-uniform temperature field induced by a localized fire. The five fire scenarios listed in Table 2 are investigated, with the main results comprising load–displacement curves and critical loads. Synthesizing the results from the five scenarios allows conclusions to be drawn regarding the influence of fire location on the buckling and post-buckling characteristics of steel dome trusses, providing a useful reference for steel structure design accounting for localized fire effects in practice.

Example 1: Truss subjected to a uniformly distributed temperature field

The steel truss considered in the first example (Figure 6) was previously studied by Yang et al. [2] under the assumption of a uniform temperature field, i.e., all members have the same temperature. The temperature levels investigated are $T = 20$ °C, 300 °C, and 500 °C, considering both elastic (EL) and elastoplastic (EP) material models. The truss has a span of $L_{truss} = 1014$ cm, a height of $H_{truss} = 184.39$, and consists of 120 identical members with a cross-sectional area $A = 0.75$ cm^2. The steel material at room temperature (T0 = 20 °C) has an elastic modulus $E_0 = 1.8 \cdot 10^4$ kN/cm^2 and a yield stress $\sigma_{y,0} = 25$ kN/cm^2.

Applying the method proposed in Section 3, the equilibrium paths are determined for the three temperature levels (Figures 7–8). For the EL model, the critical loads are $P_{cr,EL,20°C} = 10.38$ kN, $P_{cr,EL,300°C} = 8.28$ kN, and $P_{cr,EL,500°C} = 6.19$ kN. For the EP model, the corresponding values are $P_{cr,EP,20°C} = 9.95$ kN, $P_{cr,\mathrm{EP},300°C} = 8.28$ kN, and $P_{cr,\mathrm{EP},500°C} = 6.19$ kN. The obtained results agree well with those reported by Yang et al. [2], thereby confirming the correctness and reliability of the proposed nonlinear finite element method.

Example 2: Truss subjected to a localized fire

The steel truss investigated in the second example is shown in Figure 9. Its configuration and geometric parameters are similar to those of the first example, except for the cross-sectional area. All truss members are S275 steel tubes with an outer diameter $D_s = 10$ cm, an inner diameter $d_s = 9.2$ cm, and a cross-sectional area $A = 12.06$ cm^2. The truss system is connected to perimeter columns of height $H_{column} = 500$ cm, which are assumed to be protected by insulating material and thus not directly exposed to the fire. The S275 steel at room temperature ($T_0 = 20$ °C) has an elastic modulus $\mathrm{E}_0 = 2.1 \cdot 10^4$ kN/cm^2 and a yield stress $\sigma_{y,0} = 27.5$ kN/cm^2.

The fire scenario is assumed to result from a gasoline spill ignition on the floor, with a circular fire footprint of diameter $D = 2$ m and a total heat release rate $\dot{Q} = 5$ MW = 5000 kW. The fire center location is characterized by polar coordinates (r_Q, θ) as illustrated in Figure 9.

Applying the procedure proposed in Section 2, the temperature T within the truss members lying within the McCaffrey plume is determined for each fire scenario in Table 2. For each scenario, the main results, including load–displacement curves and critical loads, are presented and discussed to assess the influence of fire location on the buckling and post-buckling behavior of the steel dome truss.

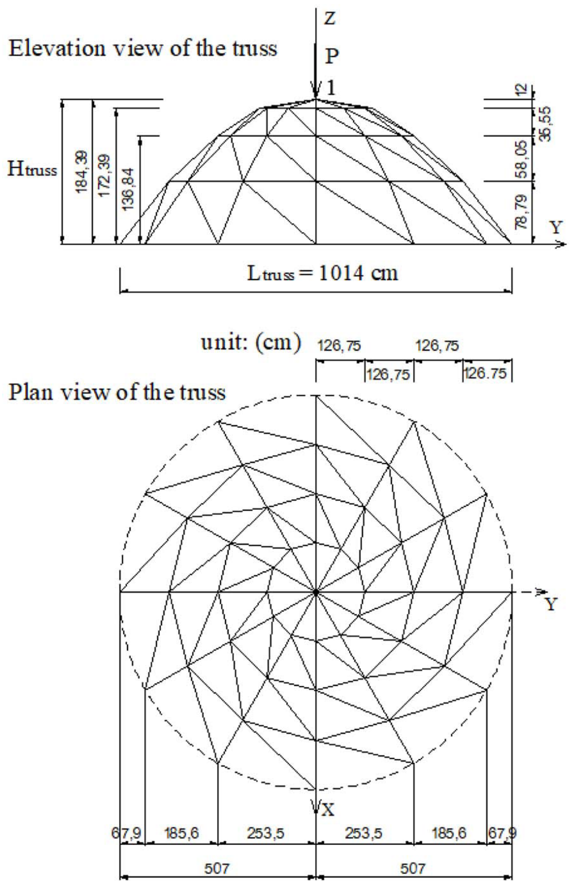

Figure 6. Latticed dome truss subjected to a uniformly distributed temperature field

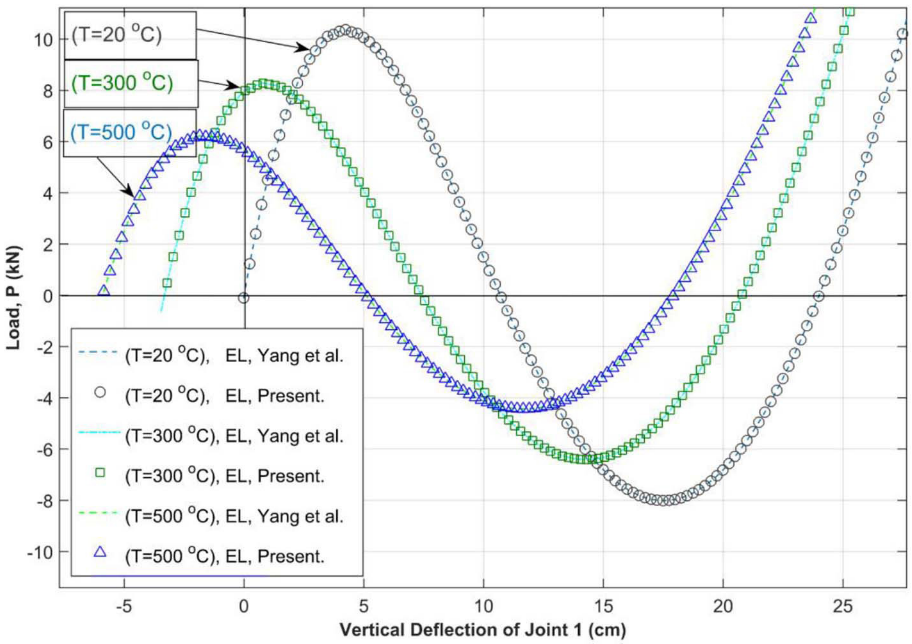

Figure 7. Load–displacement curves of the truss under a uniformly distributed temperature field (elastic material model (EL))

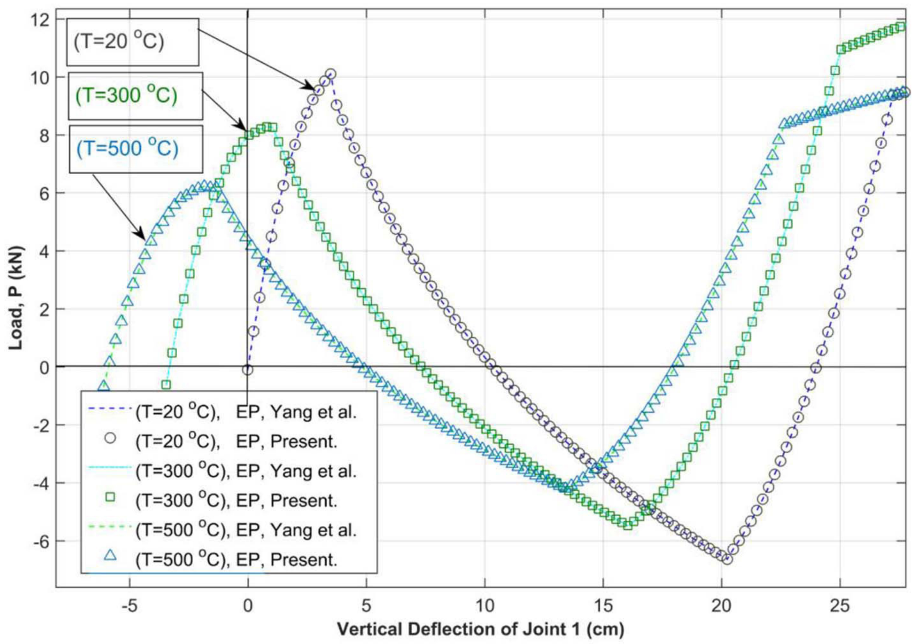

Figure 8. Load–displacement curves of the truss under a uniformly distributed temperature field (elastoplastic material model (EP))

First fire scenario: fire center at $r_Q = 0$ m

The first fire scenario (FS1) is defined with the parameters according to Table 2, specificaly-ly the fire center on the floor plan at $r_Q = 0$ m. In this scenario, the fire center coincides with the symmetry center of the truss on the floor plan, as illustrated in Figure 10. Applying the method proposed in this study, calculations are performed for both the elastic (EL) and elastoplastic (EP) models. The computed results for the two cases – (i) without fire (WF) and (ii) first fire scenario (FS1) – are shown in Figure 11.

For the no-fire case (WF), the critical load and corresponding displacement values obtained from the EL and EP analyses are as follows: *EL*:

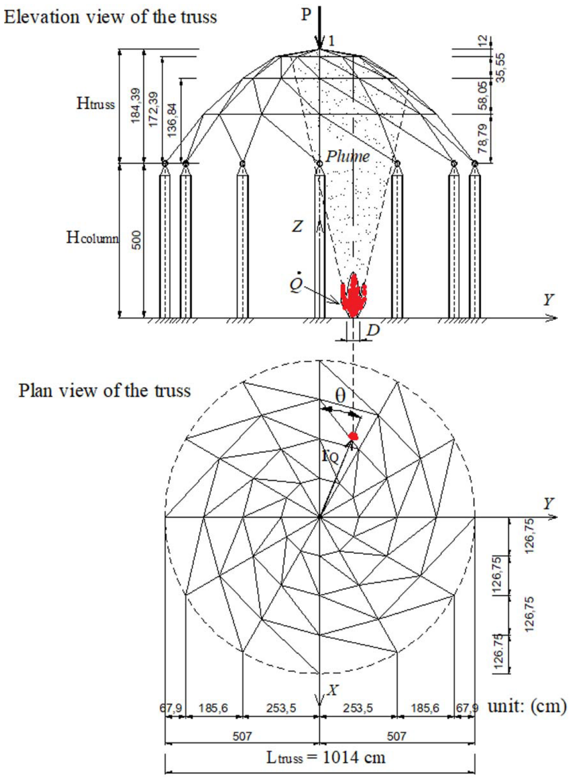

Figure 9. Steel latticed dome truss subjected to thermo-mechanical loading from a localized fire

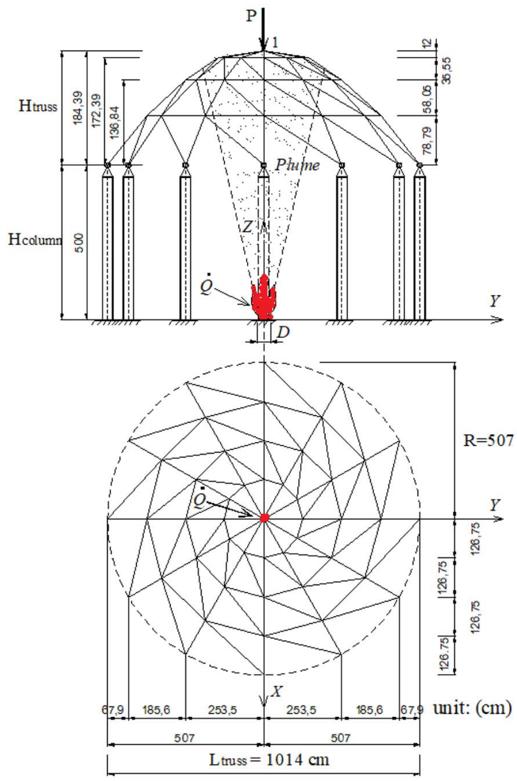

Figure 10. First fire scenario FS1 (fire center at $r_Q = 0$ m)

$\{P_{cr,EL,WF} = 193.76$ kN, $u_{cr,EL,WF} = 4.06$ cm$\}$; *EP*: $\{P_{cr,EP,WF} = 182.18$ kN, $u_{cr,EP,W} = 3.12$ cm$\}$. Similarly, for the first fire scenario: *EL*: $\{P_{cr,EL,FS1} = 405.34$ kN, $u_{cr,EL,FS1} = 1.90$ cm$\}$; *EP*: $\{P_{cr,EP,FS1} = 317.87$ kN, $u_{cr,EP,FS1} = -0.72$ cm$\}$. Figure 11 also reveals a counter-intuitive result: the critical load of the truss in scenario FS1 is higher than that in the WF case. The critical load ratios are $P_{cr,EL,FS1}/P_{cr,EL,WF} = 2.09$ and $P_{cr,EP,FS1}/P_{cr,EP,WF} = 1.74$. This phenomenon can be explained as follows. In scenario FS1, all upper chord members are subjected to the same temperature level. These members are free to expand, leading to an „arching" effect of the entire truss before the mechanical load is applied. Specifically, node 1 exhibits an upward displacement ($u_1 = -3.57$ cm) at zero load $P = 0$ (see Figure 11). This upward arching increases the effective height of the truss, thereby improving its stability and resulting in an increased critical load in this particular case.

Comment: In scenario FS1, compared to the no-fire case, the critical load increases by a factor of 2.09 in the EL analysis and 1.74 in the EP analysis. This demonstrates that a fire does not always reduce the critical load of a truss.

Second fire scenario: fire center at $r_Q = R/4$, $\theta = \pi/4$

The second fire scenario (FS2) is defined with the parameters according to Table 2, specifically the fire center on the floor plan at $r_Q = R/4$, $\theta = \pi/4$, as shown in Figure 12. Calculations are performed for both the elastic (EL) and elastoplastic (EP) models. The computed results for FS2 are shown in Figure 13.

In FS2, the critical load and displacement values obtained from the EL and EP analyses are: *EL*: $\{P_{cr,EL,FS2} = 194.65$ kN, $u_{cr,EL,FS2} = 3.31$ cm$\}$, EP: $\{P_{cr,EP,FS2} = 181.75$ kN, $u_{cr,EP,FS2} = 2.25$ cm$\}$. It can be observed that $P_{cr,EL,FS2} > P_{cr,EL,WF}$, while $P_{cr,EP,FS2} < P_{cr,EP,WF}$. Node 1 exhibits an upward displacement ($u_1 = -0.89$ cm) at zero load P = 0 (see Figure 13). Thus, the arching effect of the truss under thermal loading in FS2 tends to decrease compared to FS1. The decreasing trend of the arching effect as the fire center moves farther from the dome center will become more evident in subsequent scenarios (FS3, FS4, FS5).

Third fire scenario: fire center at $r_Q = R/2$, $\theta = \pi/4$

The third fire scenario (FS3) is defined with the parameters according to Table 2, specifically the fire center on the floor plan at $r_Q = R/2$, $\theta = \pi/4$, as

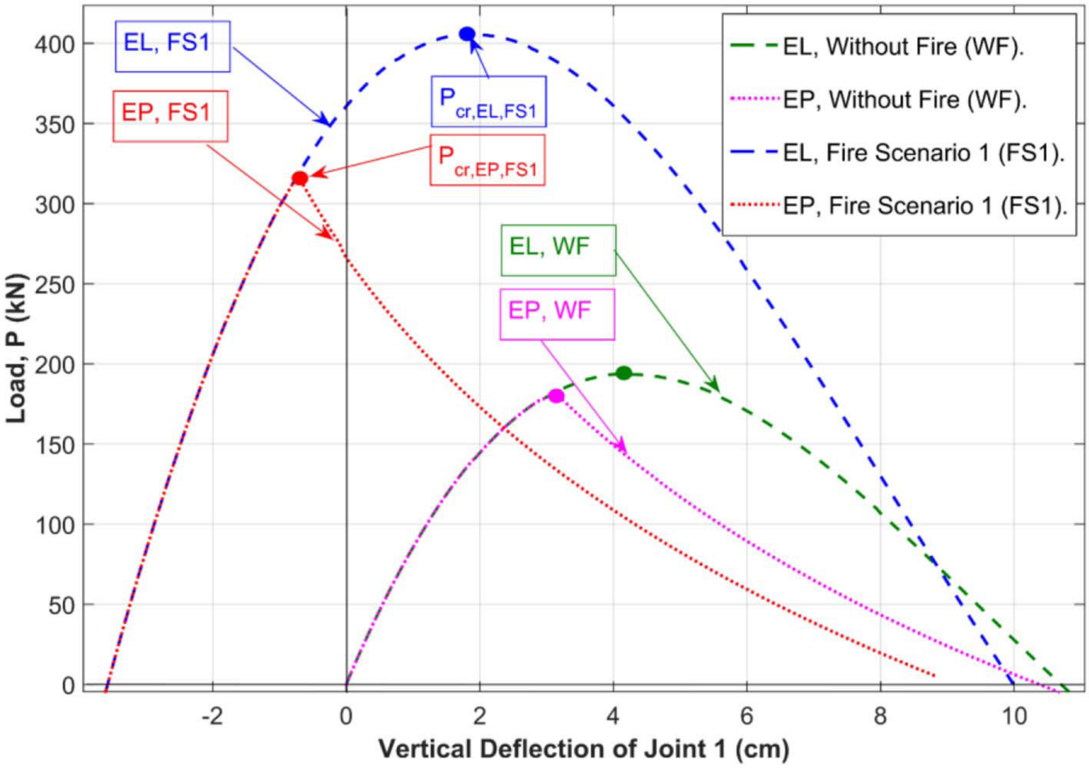

Figure 11. Load–displacement curves for two cases: FS1 and WF

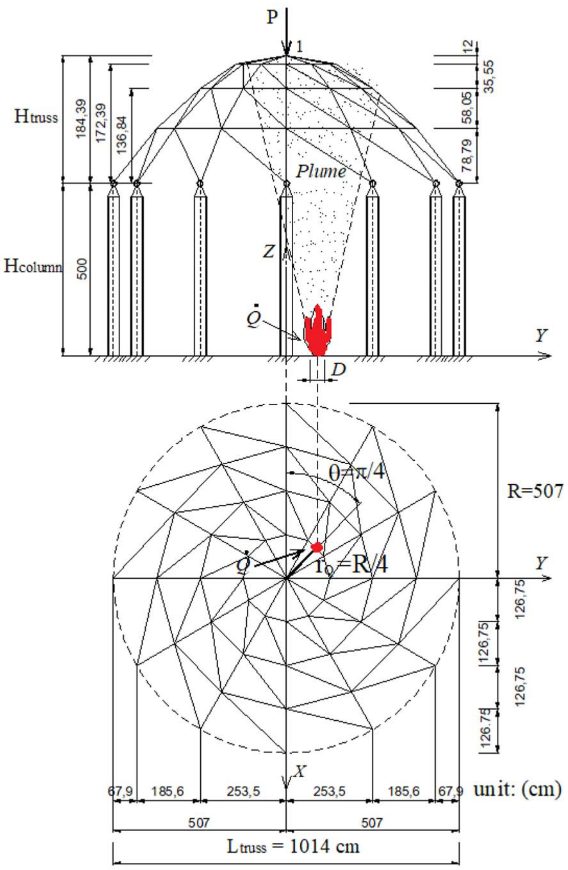

Figure 12. Second fire scenario FS2 (fire center at $r_Q = R/4$, $\theta = \pi/4$)

shown in Figure 14. Calculations are performed for both the EL and EP models. The computed results for FS3 are shown in Figure 15.

In FS3, the critical load and displacement values are: EL: $\{P_{cr,EL,FS3} = 194.51$ kN, $u_{cr,EL,FS3} = 4.15$ cm$\}$; EP: $\{P_{cr,EP,FS3} = 181.60$ kN, ucr, EP,FS3 = 2.90 cm. It can be observed that $P_{cr,EL,FS3} > P_{cr,EL,WF}$, while $P_{cr,EP,FS3} < P_{cr,EP,WF}$. Node 1 exhibits an upward displacement ($u_1 = -0.1$ cm) at zero load $P = 0$ (Figure 15). Thus, the arching effect under thermal loading in FS3 tends to decrease compared to FS2 and FS1.

Fourth fire scenario: fire center at $r_Q = 3R/4$, $\theta = \pi/4$

The fourth fire scenario (FS4) is defined with the parameters according to Table 2, specifically the fire center on the floor plan at $r_Q = 3R/4$, $\theta = \pi/4$, as shown in Figure 16. Calculations are performed for both the EL and EP models. The computed results for FS4 are shown in Figure 17.

In FS4, the critical load and displacement values are: *EL*: $\{P_{cr,EL,FS4} = 193.89$ kN, $u_{cr,EL,FS4} = 4.06$; *EP*: $\{P_{cr,EP,FS4} = 179.30$ kN, $u_{cr,EP,FS4} = 3.00$ cm$\}$. It can be observed that $P_{cr,EL,FS4} \approx P_{cr,EL,WF}$, while $P_{cr,EP,FS4} < P_{cr,EP,WF}$. Node 1 exhibits a very small upward displacement ($u_1 = -0.01$ cm) at zero load $P = 0$ (Figure 17). Thus, the arching

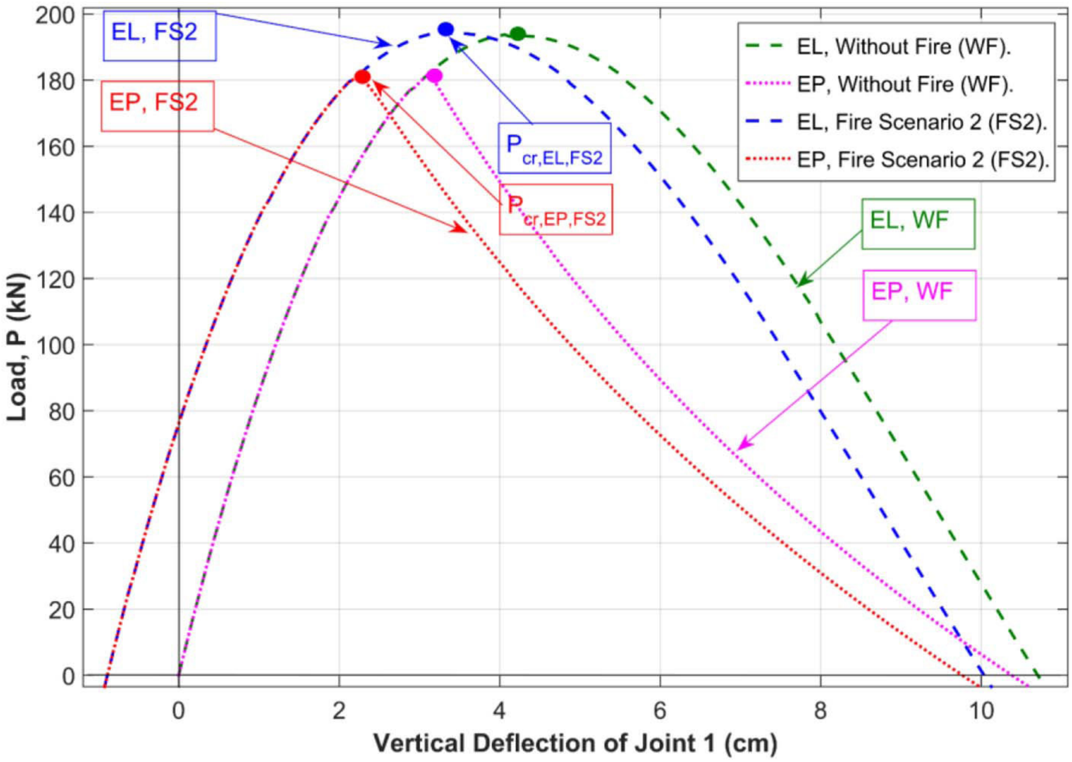

Figure 13. Load–displacement curves for two cases: FS2 and WF

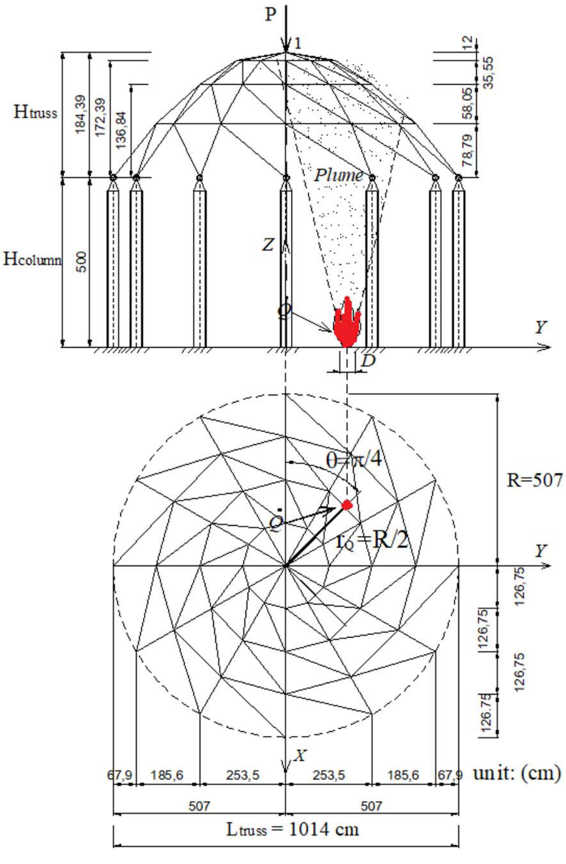

Figure 14. Third fire scenario FS3 (fire center at $r_Q = R/2$, $\theta = \pi/4$)

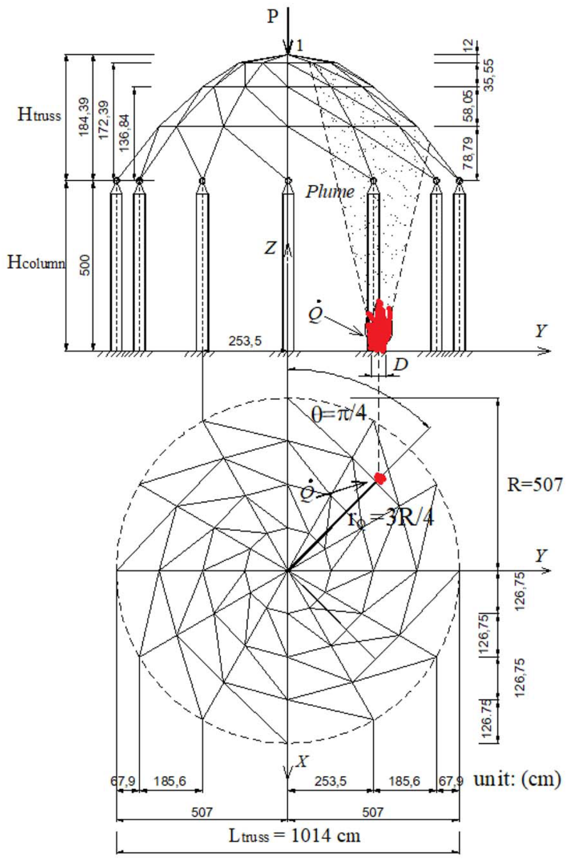

Figure 16. Fourth fire scenario FS4 (fire center at $r_Q = 3R/4$, $\theta = \pi/4$)

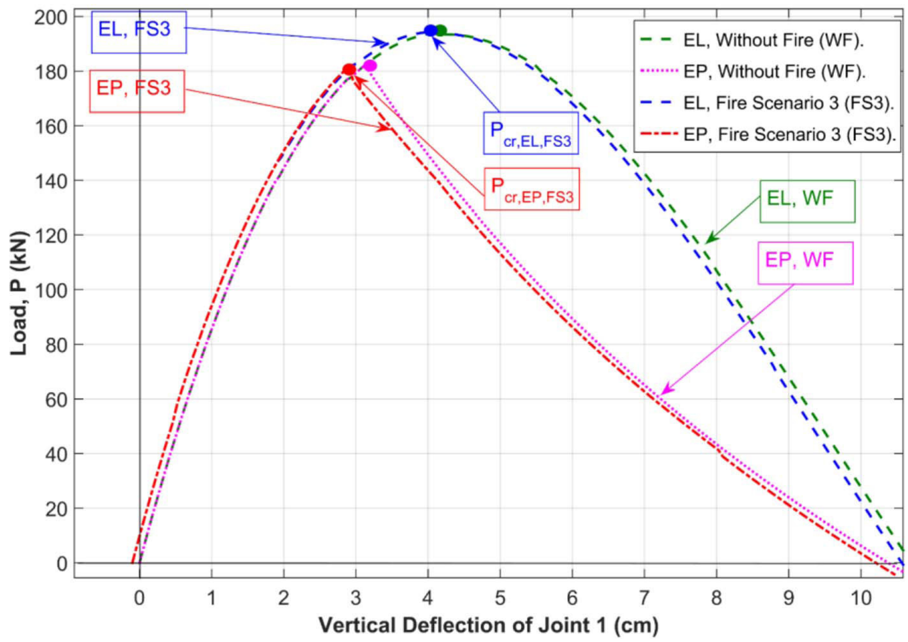

Figure 15. Load–displacement curves for two cases: FS3 and WF

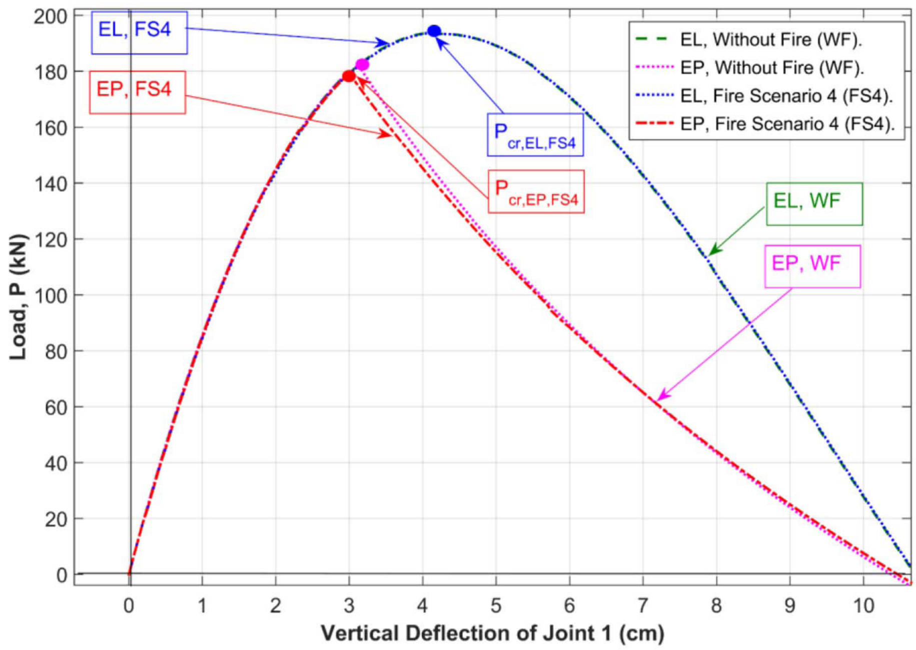

Figure 17. Load–displacement curves for two cases: FS4 and WF

effect under thermal loading in FS4 is no longer pronounced as in FS2 and FS1.

Fifth fire scenario: fire center at $r_Q = R$, $\theta = \pi/4$

The fifth fire scenario (FS5) is defined with the parameters according to Table 2, specifically the fire center on the floor plan at $r_Q = R$, $\theta = \pi/4$, as shown in Figure 18. Calculations are performed for both the EL and EP models. The computed results for FS5 are shown in Figure 19.

In FS5, the critical load and displacement values are: *EL*: $\{P_{cr,\mathrm{EL,FS5}} = 193.82$ kN, $u_{Cr,\mathrm{EL,FS5}} = 4.06$ cm$\}$; *EP*:$\{P_{cr,\mathrm{EP,FS5}} = 176.58$ kN, $u_{Cr,\mathrm{EP,FS5}} = 2.87$ cm$\}$. It can be observed that $P_{cr,\mathrm{EL,FS5}} \approx P_{cr,\mathrm{EL,WF}}$, while $P_{cr,\mathrm{EP,FS5}} < P_{cr,\mathrm{EP,WF}}$. Node 1 exhibits a negligible upward displacement (u_1 =

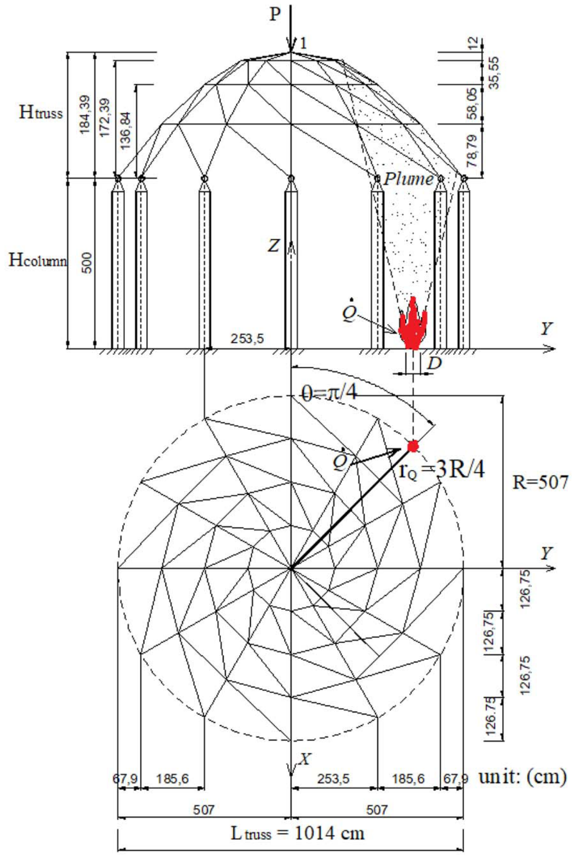

Figure 18. Fifth fire scenario FS5 (fire center at $r_Q = R$, $\theta = \pi/4$

–0.001 cm) at zero load P = 0 (Figure 19). Thus, the arching effect under thermal loading in FS5 is very small and can be neglected.

Discussion of the results in Example 2

In the second example, stability analyses of the steel truss are performed for five fire scenarios (FS1–FS5) with both material models: elastic (EL) and elastoplastic (EP). The corresponding equilibrium paths shown in Figures 11, 13, 15, 17, and 19 reveal that: (i) for the EL model, the equilibrium path exhibits no bifurcation and the critical point is a limit point; (ii) for the EP model, a bifurcation point appears.

The summarized results in Table 4 show that the critical load P_{cr} from the EP analysis is always lower than that from the EL analysis, confirming the necessity of the EP model for accurately reflecting actual structural behavior. Except for FS1, the critical loads in scenarios FS2–FS5 are all lower than those in the no-fire case (WF). Only FS1 yields a higher value due to the arching effect generated by the symmetric temperature field around the dome center. As the fire center moves outward, this arching effect diminishes and the critical load decreases, with the smallest value occurring in FS5 (fire at the dome boundary). This is the most hazardous scenario for structural stability and deserves special attention in design.

The proposed method can be extended and combined with optimization algorithms presented in [32–36] to optimize the design of steel trusses under localized fire, thereby

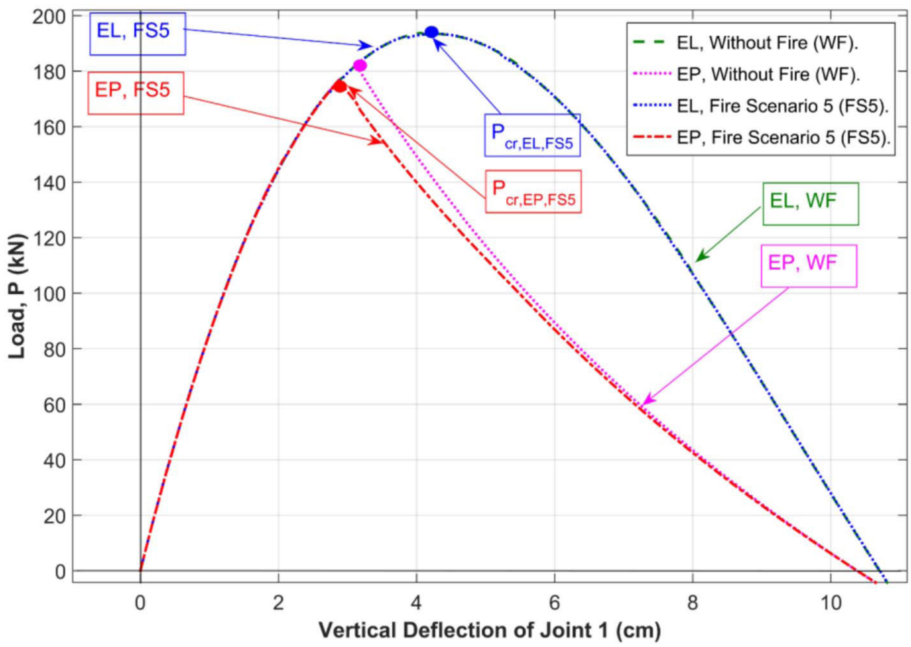

Figure 19. Load–displacement curves for two cases: FS5 and WF

Table 4. Summary of critical load and displacement results

Scenario	Fire center location (r_Q, θ)	Analysis	$P_{cr}\ (kN)$	$u_{cr}\ (cm)$
WF	—	EL	193.76	4.06
WF	—	EP	182.18	3.12
FS1	$r_Q = 0$	EL	405.34	1.90
FS1	$r_Q = 0$	EP	317.87	−0.72
FS2	$r_Q = R/4,\ \theta = \pi/4$	EL	194.65	3.31
FS2	$r_Q = R/4,\ \theta = \pi/4$	EP	181.75	2.25
FS3	$r_Q = R/2,\ \theta = \pi/4$	EL	194.51	4.15
FS3	$r_Q = R/2,\ \theta = \pi/4$	EP	181.60	2.90
FS4	$r_Q = 3R/4,\ \theta = \pi/4$	EL	193.89	4.06
FS4	$r_Q = 3R/4,\ \theta = \pi/4$	EP	179.30	3.00
FS5	$r_Q = R,\ \theta = \pi/4$	EL	193.82	4.06
FS5	$r_Q = R,\ \theta = \pi/4$	EP	176.58	2.87

contributing to improved economic efficiency and safety in practical applications. In the present study, the convergence tolerance used for the nonlinear GDC solver is set to $\|\delta \boldsymbol{U}\| / \|\boldsymbol{U}\| < 10^{-6}$. Furthermore, the current analysis assumes a steady-state temperature field (quasi-steady post-flashover condition). The McCaffrey plume equations are applied with a constant heat release rate of $\dot{Q}$ = 5 MW. A time-dependent (transient) analysis is recommended for future extensions of this work. The truss is connected to perimeter columns, which are assumed to have no horizontal displacement; thus, the truss is considered to have fixed supports at the boundary. The McCaffrey model is empirical, with a typical uncertainty of approximately ±10–15% in the centerline temperature [25]; this uncertainty has not been considered in the present study and is recommended for future investigations.

The validation in the present study is limited to the case of a uniformly distributed temperature field [2], due to the lack of publicly available experimental data on steel dome trusses under localized fire that includes complete post-buckling response. Nevertheless, the McCaffrey fire plume model has been independently validated for temperature field predictions in fire safety engineering [25], and the structural solver used herein has been validated through Example 1. Consequently, the reliability of the proposed model for localized fire exposure is considered justifiable within the scope of this study.

CONCLUSIONS

This paper has developed a comprehensive nonlinear finite element framework for evaluating the buckling and post-buckling response of latticed steel dome trusses subjected to combined mechanical loads and non-uniform temperature fields induced by localized fires. Based on the presented numerical results, the following main conclusions can be drawn:

1. The thermo-mechanical problem of steel trusses under localized fire belongs to the weak coupling class, allowing a sequential solution strategy: the temperature field is first determined from the McCaffrey plume model and then used as thermal loading input for the mechanical problem. This approach achieves a favorable balance between accuracy and computational efficiency.
2. The combination of the McCaffrey plume model (determining centerline temperature with height across three zones) and a Gaussian lateral distribution enables a practical description of the three-dimensional temperature field induced by a localized fire. The parameterization method using polar coordinates (r_Q, θ) allows systematic investigation of the influence of fire location on structural stability.
3. The truss element formulation based on the UL method with Green's strain accounts for large displacements (geometric nonlinearity), temperature-dependent thermal expansion, and degradation of steel mechanical properties with temperature according to Eurocode 3 (for both elastic and elastoplastic models).

The GDC method enables tracing of the entire equilibrium path including critical points and post-buckling response.
4. The analysis results for the latticed dome truss subjected to a uniformly distributed temperature field (Example 1) agree well with the published results of Yang et al. [2], confirming the reliability of the proposed finite element model and algorithm.
5. The parametric study with five fire scenarios (FS1–FS5) on an S275 steel tubular truss reveals that: (i) When the fire is exactly at the symmetric center (FS1, $r_Q = 0$): the critical load increases significantly (by a factor of 2.09 for the elastic analysis and 1.74 for the elastoplastic analysis) compared to the no-fire case. This is due to the arching effect caused by symmetric thermal expansion of the upper chord members, which increases the effective height of the truss; (ii) As the fire moves away from the center: the arching effect gradually diminishes (evidenced by the displacement at node 1 at $P = 0$ decreasing from -3.57 cm in FS1 to -0.001 cm in FS5); (iii) The most hazardous scenario is FS5 (fire at the dome boundary, $r_Q = R$): the critical load in the elastoplastic analysis decreases by approximately 4% (from 182.18 kN to 176.58 kN) compared to the no-fire case, with no significant arching effect; (iv) The elastoplastic analysis consistently yields lower critical loads than the elastic analysis (by 2% to 22% depending on the scenario), confirming the necessity of considering material nonlinearity to accurately reflect the actual behavior of steel structures under fire conditions.
6. The finding that a fire at the dome boundary is more hazardous than a fire at the dome center is contrary to conventional intuition but has a clear physical basis. This provides important guidance for performance-based fire design of large-span steel dome trusses. Engineers should pay particular attention to potential fire scenarios at the boundary regions of such structures.

REFERENCES

1. Yang, Y.B., Lin, T.J.and Leu, L.J. Thermal effect on the postbuckling behavior of an elastic or elastoplastic truss. Journal of Engineering Mechanics, 2008; 134(4): 330–338.
2. Yang, Y.B., et al., Inelastic postbuckling response of steel trusses under thermal loadings. Journal of Constructional Steel Research, 2008; 64(12): 1394–1407.
3. Dao, Ngoc T., et al., Thermomechanical buckling and postbuckling of steel trusses with initial load and length imperfection. The Structural Design of Tall and Special Buildings, 2025; 34(9): e70045.
4. Jiang, S., et al., Full-scale fire tests on steel roof truss structures. Journal of Constructional Steel Research, 2020; 169: 106025.
5. Sibil, R. and Ozyurt, E. A Numerical study to evaluate the changes in dynamic properties of various steel truss types under fire conditions. International Journal of Steel Structures, 2023; 23(6): 1476–1489.
6. Chen, C.-k. and Zhang, W. Structural behaviors of steel roof truss exposed to pool fire. Journal of Central South University, 2012; 19(7): 2054–2060.
7. Chen, C.-k. and Zhang, W. Comparative experimental investigation on steel staggered-truss constructed with different joints in fire. Journal of Constructional Steel Research, 2012; 77: 43–53.
8. Ozyurt, E. and Wang, Y.C. Effects of non-uniform temperature distribution on critical member temperature of steel tubular truss. Engineering Structures, 2016; 116: 95–106.
9. Rezaiee-Pajand, M., Masoodi A.R., Arabi, E. Geometric and material nonlinear analyses of trusses subjected to thermomechanical loads. Structural Engineering International, 2023; 33(2): 302–313.
10. Pham, V.D., et al., Large-deflection analysis of eccentrically compressed beams under thermal effects: a least-squares optimization framework. ZAMM - Journal of Applied Mathematics and Mechanics / Zeitschrift für Angewandte Mathematik und Mechanik, 2026; 106(4): e70388.
11. Dao, N.T. and Tran Thi, T.V. Mixed finite element formulation in nonlinear geometrical analysis of space trusses and application to trusses with member length imperfection. Journal of Computing and Information Science in Engineering, 2024; 25(1).
12. Dao, N.T. and Thi, T.V.T. Hybrid finite element method in nonlinear dynamic analysis of trusses. International Journal of Structural Stability and Dynamics, 2023; 23(20): 2450195.
13. Pham, V.D., et al., The effect of support stiffness on buckling and post-buckling of imperfect plane arch trusses. Mechanics of Solids, 2024; 59(6): 3656–3672.
14. Van Dat, P., et al., Investigating the impact of spring support stiffness on dynamic buckling of imperfect steel trusses. Results in Engineering, 2025; 25: 104490.
15. Dao, N.T., Van Tran Thi, T. and Cuong-Le, T. A new stochastic global algorithm for critical load optimization of dome trusses. Optimization and Engineering, 2025; 26(2): 1143–1202.
16. Eurocode 3, d.o.s.s., part 1.2, Structural fire design.

European Committee for Standardization, 1993.

17. Ma, C., Yan, X. and Gernay, T. 4 - Properties of cold-formed steels exposed to elevated temperatures, in Construction Materials and Their Properties for Fire Resistance and Insulation, P.O. Awoyera and M.Z. Naser, Editors. 2025, Woodhead Publishing. p. 59–78.
18. Bączkiewicz, J., et al., Experimental study on axially loaded square hollow section T-joints under fire conditions. Fire Safety Journal, 2020; 114: 102993.
19. Bączkiewicz, J., et al., Parametric study on axially loaded square hollow section T-joints at elevated temperature. Fire Safety Journal, 2021; 122: 103359.
20. Jeanneret, C., et al. Chord Shielding Effect in Steel Trusses When Exposed to a Localized Fire. in Proceedings of the Canadian Society for Civil Engineering Annual Conference 2023, Volume 11. 2024. Cham: Springer Nature Switzerland.
21. Kallada Janardhan, R., et al., Coupled CFD-FE analysis of a long-span truss beam exposed to spreading fires. Engineering Structures, 2022; 259: 114150.
22. Couto, C., Vila Real, P. and Lopes, N. Local-global buckling interaction in steel I-beams—A European design proposal for the case of fire. Thin-Walled Structures, 2025; 206: 112664.
23. Stochino, F., et al., Fire-induced structural failure analysis of an industrial warehouse roof truss system. Procedia Structural Integrity, 2024; 64: 1782–1789.
24. Mccaffrey, B.J. Purely buoyant diffusion flames: some experimental results. 1979.
25. Karlsson, B., J. Quintiere, and N. Johansson, Enclosure Fire Dynamics. 2022.
26. Peacock, R., et al., A User's Guide for FAST: Engineering Tools for Estimating Fire Growth and Smoke Transport. 2000, Special Publication (NIST SP), National Institute of Standards and Technology, Gaithersburg, MD.
27. McGrattan, K., et al., Fire Dynamics Simulator, Technical Reference Guide, Sixth Edition. 2013, Special Publication (NIST SP), National Institute of Standards and Technology, Gaithersburg, MD.
28. Manual of steel construction: Load and resistance factor design. Structural members, specification and codes, 2nd ed. vol. 1. Chicago (IL): American Institute of Steel Construction. 1994.
29. Leon, S.E., et al., A unified library of nonlinear solution schemes. Applied Mechanics Reviews, 2012; 64(4).
30. Crisfield, M.A., A fast incremental/iterative solution procedure that handles "snap-through". Computers & Structures, 1981; 13(1): 55–62.
31. Bellini, P.X. and Chulya, A. An improved automatic incremental algorithm for the efficient solution of nonlinear finite element equations. Computers & Structures, 1987; 26(1): 99–110.
32. Alyafei, H.F.S., et al., AI-driven multi-parameter optimization of high-performance epoxy composites for tribological applications. Advances in Science and Technology Research Journal, 2026; 20(7).
33. Zheng, S.Q., Liu, X. and Zhao, M. Integrated design and multi-objective optimization of lightweight brake system for a Formula Student racing car. Advances in Science and Technology Research Journal, 2026; 20(6): 273–285.
34. Mustaffa, E.M.M., et al., A dual-response optimization framework for fused deposition modeling printed polyethylene terephthalate glycol: Integrating surface finish and tensile-yield strength via response surface methodology. Advances in Science and Technology Research Journal, 2026; 20(6): 247–261.
35. Zhu, Z., et al., Path planning optimization of automated guided vehicles based on enhanced A* and dynamic window approach fusion algorithms. Advances in Science and Technology Research Journal, 2026; 20(5): 521–534.
36. Balasa, R.K., Veera, M.R. and Battula, T.K. Interference-resilient design of aperiodic phased arrays for 5G applications using modified Laplacian invasive weed optimization. Advances in Science and Technology Research Journal, 2026; 20(5): 386–399.